

A Comparative Molecular Field Analysis Model for 6-Arylpyrrolo[2,1-*d*][1,5]benzothiazepines Binding Selectively to the Mitochondrial Benzodiazepine Receptor

Giovanni Greco,[§] Ettore Novellino,^{*,§} Isabella Fiorini,^{||} Vito Nacci,^{||} Giuseppe Campiani,^{||} Silvia M. Ciani,^{||} Antonio Garofalo,^{||} Paola Bernasconi,[†] and Tiziana Mennini[‡]

Dipartimento di Chimica Farmaceutica e Tossicologica, Università di Napoli "Federico II", Via D. Montesano 49, 80131 Napoli, Italy, Dipartimento Farmaco Chimico Tecnologico, Università di Siena, Via Banchi di Sotto 55, 53100 Siena, Italy, and Istituto di Ricerche Farmacologiche "Mario Negri", Via Eritrea 62, 20157 Milano, Italy

Received June 15, 1994[®]

A series of 42 6-arylpyrrolo[2,1-*d*][1,5]benzothiazepines, which we have recently described as selective ligands of the mitochondrial benzodiazepine receptor (MBR) (Fiorini I.; *et al.* *J. Med. Chem.* **1994**, *37*, 1427–1438), have been investigated using the comparative molecular field analysis (CoMFA) approach. The resulting 3D-QSAR model rationalizes the steric and electronic factors which modulate affinity to the MBR with a cross-validation standard error of 0.648 pIC₅₀ unit. A set of seven novel pyrrolobenzothiazepine congeners has successively been synthesized and tested. The CoMFA model forecasts the binding affinity values of these new compounds with a prediction standard error of 0.536.

Introduction

During the past decade, the mitochondrial benzodiazepine receptor (MBR)^{1,8} has been the object of several studies aimed to understand its physiological role^{9–22} and to establish structure–activity relationships for ligands to which it binds selectively.^{11,22–27} Among the many investigated cellular functions of this receptor, its role in the CNS appears particularly interesting for possible therapeutical applications. It has in fact been hypothesized that occupation of the MBR by agonists stimulates steroidogenesis in glial cells by promoting the transport of cholesterol into mitochondrial membranes.^{18–20} As a consequence, more cholesterol would be converted into neurosteroids^{28–30} such as pregnenolone sulfate, dehydroepiandrosterone sulfate, 3 α -hydroxy-5 α -pregnan-20-one, and 3 α ,21-dihydroxy-5 α -pregnan-20-one. By interacting with the γ -aminobutyric acid (GABA) receptor–chloride ionophore complex,³¹ the above neurosteroids would therefore control the sensitivity of this receptor complex to the natural agonist, GABA.^{21,22}

The following are the most well-known ligands of the MBR which have more frequently been employed as pharmacological probes: alpidem,³² Ro 5-4864,³³ and PK 11195.^{34,35} In addition to these compounds, a series of 2-arylindol-3-acetamides binding selectively to the MBR and displaying "antineophobic" effects in animal experiments have recently been reported by Kozikowski and co-workers.²²

In a previous paper,²⁷ we described the synthesis and the biological evaluation of a set of 6-arylpyrrolo[2,1-*d*][1,5]benzothiazepines binding with high specificity to the MBR. Moreover, through molecular modeling, we have tried to establish the receptor-recognized conformations of the investigated ligands as well as a qualitative correlation between their potency and stereoelectronic properties.

Here we present the development of a three-dimensional quantitative structure–activity relationship (3D-QSAR) based on the same data set using the comparative molecular field analysis (CoMFA) method.³⁶ In order to better assess the robustness of the derived 3D-QSAR, a new series of seven pyrrolobenzothiazepines has been synthesized and the observed binding affinity values have been compared with those forecasted by the CoMFA model.

3D-QSAR Methods

Biological Data. The structures and the binding affinity values of the compounds forming the training set (1–42) are listed in Table 1. The end point being modeled is the pIC₅₀ of the ligands, that is, the -log of the molar concentration of compound required to displace the specific binding of [³H]PK 11195 by 50%.²⁷

Table 2 lists the structures and the biological data of seven pyrrolobenzothiazepine derivatives (62–68) which were newly synthesized and submitted to binding assay under the same conditions²⁷ (see the Experimental Section). Since these ligands have been used to test the predictive ability of the CoMFA model derived from the training set, they constitute what we have called the test set.

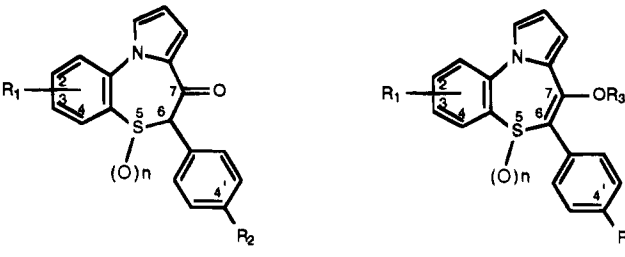
Several pIC₅₀ values listed in Table 1 are characterized by some uncertainty as they refer to racemic mixtures (1–7) or to "inactive" compounds (6, 19, 25, 39, 40, and 42) for which the pIC₅₀ values are all below the threshold value of 4.00. Although such data might represent a disturbing source of noise, it is also true that the exclusion of a non-negligible number of observations would imply a serious loss of information. Thus, the above compounds have been included, as a first approximation, in the CoMFA study with pIC₅₀ values of 4.00. There are examples in literature where analogous decisions have been taken in dealing with "truncated" activity values³⁶ or diastereomeric mixtures.³⁷ Concerning compounds 1–7, these were modeled as *S*-enantiomers because in such a configuration they fitted better our proposed pharmacophoric model.²⁷

[§] Dipartimento di Chimica Farmaceutica e Tossicologica, Napoli.

^{||} Dipartimento Farmaco Chimico Tecnologico, Siena.

[†] Istituto di Ricerche Farmacologiche "Mario Negri", Milano.

[®] Abstract published in *Advance ACS Abstracts*, October 1, 1994.

Table 1. Affinity Values for [³H]PK 11195 Binding Inhibition of the Compounds Forming the "Training Set"


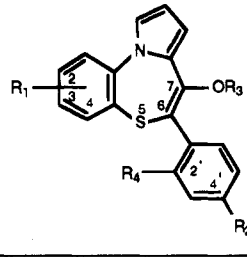
compd	R ₁	R ₂	n	R ₃	pIC ₅₀		
					obsd ^a	pred ^b	calcd ^c
1	H	H	0		5.91	5.50	5.84
2	H	OCH ₃	0		5.68	6.08	5.95
3	2-CF ₃	OCH ₃	0		5.21	5.39	5.20
4	2-Cl	OCH ₃	0		5.85	5.66	5.86
5	H	H	1		4.83	4.30	4.51
6	H	H	2		4.00	5.01	4.12
7	H	OCH ₃	1		4.64	4.77	4.58
8	H	H	0	SO ₂ CH ₃	7.24	7.46	7.53
9	H	H	0	COCH ₃	7.71	6.99	7.17
10	H	H	0	COC ₂ H ₅	7.18	7.26	7.33
11	H	H	0	CO- <i>n</i> -C ₃ H ₇	7.67	7.60	7.67
12	H	H	0	CO- <i>n</i> -C ₄ H ₉	7.32	7.53	7.70
13	H	H	0	CO- <i>n</i> -C ₅ H ₁₁	7.63	7.70	7.72
14	H	H	0	CON(CH ₃) ₂	8.04	7.59	7.98
15	H	OCH ₃	0	CO- <i>n</i> -C ₃ H ₇	7.56	7.28	7.60
16	2-CF ₃	OCH ₃	0	COCH ₃	5.34	5.43	5.20
17	2-CF ₃	OCH ₃	0	COC ₂ H ₅	5.53	6.03	5.50
18	2-CF ₃	OCH ₃	0	CON(CH ₃) ₂	6.53	5.69	5.93
19	2-CF ₃	OCH ₃	0	COC ₆ H ₂ -3,4,5-(OMe) ₃	4.00	2.97	3.50
20	2-Cl	H	0	COCH ₃	6.25	6.47	6.48
21	2-Cl	H	0	COC ₂ H ₅	6.09	6.89	6.65
22	2-Cl	OCH ₃	0	COCH ₃	6.19	6.28	6.18
23	2-Cl	OCH ₃	0	COC ₂ H ₅	6.31	6.90	6.41
24	2-Cl	OCH ₃	0	CON(CH ₃) ₂	6.78	6.81	6.80
25	2-Cl	OCH ₃	0	COC ₆ H ₂ -3,4,5-(OMe) ₃	4.00	4.01	4.11
26	3-Cl	H	0	COCH ₃	6.64	6.95	6.87
27	3-Cl	OCH ₃	0	COCH ₃	6.62	6.47	6.56
28	4-Cl	H	0	COCH ₃	8.12	7.39	7.84
29	4-Cl	OCH ₃	0	COCH ₃	7.69	7.16	7.53
30	2-OCH ₃	OCH ₃	0	COCH ₃	5.74	6.42	5.96
31	H	H	1	COCH ₃	6.16	6.23	6.12
32	H	H	2	COCH ₃	5.94	6.31	5.99
33	H	OCH ₃	1	COCH ₃	5.68	5.93	5.83
34	H	OCH ₃	2	COCH ₃	6.20	5.46	5.69
35	H	OCH ₃	1	COC ₃ H ₇	6.57	6.49	6.48
36	H	OCH ₃	0	CON(CH ₃) ₂	8.04	7.02	7.51
37	H	OCH ₃	0	COCH ₃	7.47	6.91	7.06
38	H	OCH ₃	0	SO ₂ CH ₃	7.02	7.30	7.29
39	H	OCH ₃	0	CO-3-pyridyl	4.00	5.79	4.44
40	H	OCH ₃	0	COC ₆ H ₂ -3,4,5-(OMe) ₃	4.00	5.44	4.99
41	H	OCH ₃	0	COC ₂ H ₅	7.53	6.99	7.37
42	H	OCH ₃	0	CO-4-pyridyl	4.00	4.84	3.81

^a Data taken from ref 27. ^b Values predicted in the cross-validation run. ^c Values calculated according to the calibration model.

Molecular Conformation and Superimposition.

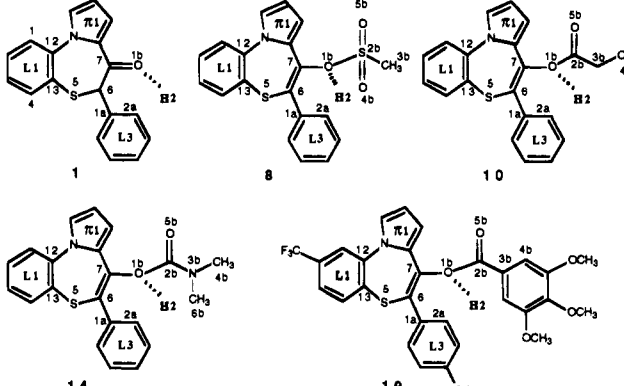
The geometries of the compounds were modeled with standard bond distances and angles using SYBYL³⁸ and energy-minimized with the Tripos force field³⁹ with neglect of electrostatics. Detailed molecular modeling procedures can be found in our previous publication.²⁷ Table 3 lists the torsional angles defining the bioactive conformations of compounds **1**, **8**, **10**, **14**, and **19**, chosen as representative of other closely related analogs.

Concerning the alignment rule, we used geometries resulting from an already described superimposition of the ligands on the template Ro 5-4864.²⁷ The various

Table 2. Affinity Values for [³H]PK 11195 Binding Inhibition of the Compounds Forming the "Test Set"


compd	R ₁	R ₂	R ₃	R ₄	IC ₅₀ ± SE ^a	pIC ₅₀		obsd ^b
						obsd ^b	pred ^c	
62	H	H	COCH ₃	F	38 ± 6	7.42	7.24	0.18
63	H	H	CON(CH ₃) ₂	F	31 ± 4	7.51	8.06	-0.55
64	H	Cl	COCH ₃	H	30 ± 3	7.52	6.82	0.70
65	H	F	COCH ₃	H	28 ± 3	7.55	6.85	0.70
66	2-CH ₃	H	COCH ₃	H	675 ± 75	6.17	6.93	-0.76
67	3-CH ₃	H	COCH ₃	H	112 ± 21	6.95	7.19	-0.24
68	4-Cl	H	CON(CH ₃) ₂	H	4 ± 0.4	8.40	8.64	-0.24
PK 11195 ^d					2 ± 0			

^a Experimental IC₅₀ values (nM). ^b Experimental pIC₅₀ values. ^c pIC₅₀ values predicted through the CoMFA calibration model derived from compounds **1**–**42**. ^d The IC₅₀ value of PK 11195 is reported only as a reference.

Table 3. Conformations of a Subset of Ligands^a


compd	τ ₁ (deg)	τ ₂ (deg)	τ ₃ (deg)	τ ₄ (deg)	τ ₅ (deg)
1 ^b	-9.5				-69.6
8	-42.2	167.6	-157.0		-69.6
10	-45.9	167.2	173.2	60.9	-71.2
14	-45.9	166.9	174.3	180.0	-72.1
19	-45.0	170.0	172.9	-168.4	-70.9

^a τ₁ = τ(C2a,C1a,C6,C7); τ₂ = τ(C6,C7,O1b,X2b); τ₃ = τ(C7,O1b,X2b,X3b); τ₄ = τ(O1b,X2b,X3b,C4b); τ₅ = τ(C12,C13,S5,C6). ^b Compounds **1**–**7** were modeled as *S*-enantiomers because of their better fit into the pharmacophore model (see ref 27).

compounds (training set and test set) overlap at the following pharmacophore points (see labels in Table 3): (1) the centroid L1 of the fused benzene ring, (2) the centroid L3 of the pendant phenyl ring, (3) the lone pair H2 elongated up to 2.0 Å from a carbonyl or an ester oxygen along an ideal hydrogen-bond geometry, and (4) the centroid π1 of the pyrrole moiety.

The compounds of the test set were modeled analogously to those of the training set. Actually, for **62** and **63** there were two alternative ways to orient the 2'-fluoro group, depending on whether the fluorine atom pointed toward (conformation A) or away from (conformation B) the endo-cyclic sulfur. The two conformations did not show appreciable differences in steric energy (less than 0.1 kcal/mol) according to molecular mechanics (Tripos) and semiempirical quantummechanics (MO-

PAC⁴⁰/MNDO⁴¹) calculations. However, the CoMFA electrostatic contour maps relative to the training set (see below) suggested that the latter type of orientation was to be preferred. This was confirmed by the fact that orientation B was predicted for both compounds with significantly higher pIC₅₀ values (the differences being about 0.7 unit).

CoMFA Calculations. CoMFA was carried out using the QSAR option of SYBYL. The partial atomic charges used in CoMFA were computed using the MNDO semiempirical model available in the MOPAC program. Single-point calculations were performed on the geometries previously optimized with SYBYL/MAXIMIN2.

The steric and electrostatic probe–ligand interaction energies (kcal/mol) were calculated with the Lennard–Jones and Coulomb potential functions of the Tripos force field using a C_{sp}³ probe atom carrying a charge of 1.0. The steric and electrostatic energies were truncated at 5.0 and 30 kcal/mol, respectively; the electrostatic ones were not dropped in correspondence of lattice points inside the union volume of the superimposed ligands.

The dimensions of the CoMFA lattice were determined through an automatic procedure, featured by the SYBYL/CoMFA routine, which extends the lattice walls beyond the dimensions of each structure by 4.0 Å in all directions. The lattice spacing was set to a value of 2.0 Å.

PLS Regression Analysis. All the calculations were performed with the SYBYL/QSAR routine. The partial least squares (PLS) regression analysis⁴² on the training set of 42 compounds was carried out on a subset of steric and electrostatic energy parameters characterized by a standard deviation not lower than 1.0 kcal/mol. This way, the number of energy variables was reduced from a total of 2420 down to 354 (122 steric and 232 electrostatic). The steric and electrostatic fields were subjected to scaling in order to assign them the same weight (the command “scaling CoMFA–std” was used).

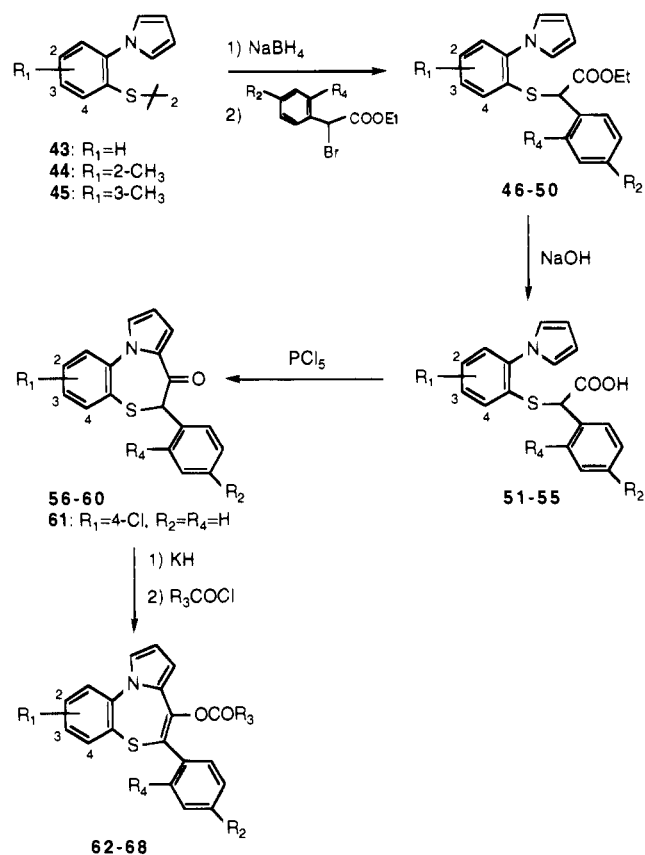
The cross-validation procedure⁴³ was performed by dividing the training set into 10 randomly selected groups. The optimal number of latent variables was that of the cross-validation equation with the lowest standard error and a significance level, estimated by means of the stepwise *F*-test, not lower than 99.5%.

After the optimal dimensionality of each model was established, the corresponding calibration equation (resulting from the simultaneous contribution of all the observations) was derived. The calibration equation with latent variables was then converted into the original parametric space represented by probe–ligand interaction energies; a 3D-QSAR was therefore derived whose coefficients were associated with statistically significant lattice locations. CoMFA coefficient contour maps were generated by interpolation of the pairwise products between the 3D-QSAR coefficients and the standard deviations of the associated energy variables. The derived 3D-QSAR calibration model was successively employed to forecast the binding affinity values of the seven compounds listed in Table 2.

Chemistry

Convenient access to the target derivatives **62–68** (Table 2) was gained by a previously reported general

Scheme 1

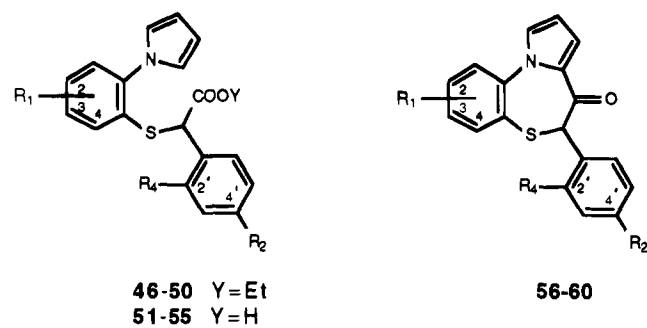


synthetic route²⁷ (see Scheme 1). Compounds **44** and **45** were obtained from the proper bis(2-aminophenyl) disulfides and dimethoxytetrahydrofuran.^{44,45} The reduction–alkylation reaction of **43**^{46–45} afforded **46–50** using NaBH₄ as reducing agent and ethyl α-bromoacetates (prepared by usual way²⁶). Hydrolysis of **46–50** gave acids **51–55** which were cyclized to **56–60** with PCl₅. Ketones **56–60** and **61**²⁷ were converted to the target compounds **62–68** using KH as enolizing agent and the selected acyl chlorides. Physicochemical data of intermediates **46–60** are listed in Table 4.

Results and Discussion

CoMFA in the Training Set. The statistics of the PLS regression analysis applied on the training set data are reported in Table 5 (the legend of this table defines statistical parameters which are mentioned below). The stepwise *F*-test performed on the PRESS values (cross-validation) justifies four components with an *s*_{cv} of 0.648 and an *r*²_{cv} of 0.764. Expectedly, the corresponding calibration model yields a better data fitting (*s*_f = 0.330 and *r*²_f = 0.939). Observed, predicted, and calculated pIC₅₀ values are listed in Table 1 and plotted in Figure 1.

In order to visualize the information content of the derived 3D-QSAR model, CoMFA contour maps were generated by interpolating the products between the 3D-QSAR coefficients and their associated standard deviations. It is worthwhile to remark that these types of contours can be found only in the corresponding areas of the lattice points characterized by variance of the steric and electrostatic properties of the ligands. Thus, their absence does not necessarily mean that a given pharmacophoric element is actually unimportant but

Table 4. Physicochemical Data of Intermediates 46–60

compd	R ₁	R ₂	R ₄	% yield	recryst solv ^a	mp, °C	formula
46	H	H	F	66		<i>b</i>	C ₂₀ H ₁₈ FNO ₂ S
47	H	Cl	H	57		<i>b</i>	C ₂₀ H ₁₈ ClNO ₂ S
48	H	F	H	53		<i>b</i>	C ₂₀ H ₁₈ FNO ₂ S
49	2-CH ₃	H	H	50	A	75–76	C ₂₁ H ₂₁ NO ₂ S
50	3-CH ₃	H	H	72		<i>b</i>	C ₂₁ H ₂₁ NO ₂ S
51	H	H	F	73	B	44–46	C ₁₈ H ₁₄ FNO ₂ S
52	H	Cl	H	47		<i>b</i>	C ₁₈ H ₁₄ ClNO ₂ S
53	H	F	H	95		<i>b</i>	C ₁₈ H ₁₄ FNO ₂ S
54	2-CH ₃	H	H	56	B	125–128	C ₁₉ H ₁₇ NO ₂ S
55	3-CH ₃	H	H	72		<i>b</i>	C ₁₉ H ₁₇ NO ₂ S
56	H	H	F	67	A	152–153	C ₁₈ H ₁₂ FNOS
57	H	Cl	H	48	A	162–163	C ₁₈ H ₁₂ ClNOS
58	H	F	H	72	A	153–155	C ₁₈ H ₁₂ FNOS
59	2-CH ₃	H	H	48	A	119–120	C ₁₉ H ₁₅ NOS
60	3-CH ₃	H	H	34		<i>b</i>	C ₁₉ H ₁₅ NOS

^a Recrystallization solvent: A = ethanol; B = cyclohexane.
^b Thick oil.

Table 5. Statistics of the CoMFA Model Derived from Compounds 1–42^a

LV	cross-validation			calibration	
	s _{CV}	r ² _{CV}	F _{1,k}	s _f	r ² _f
1	1.050	0.330	19.701	0.925	0.480
2	0.912	0.507	14.021	0.757	0.661
3	0.812	0.620	11.197	0.514	0.847
4 ^b	0.648	0.764	22.670	0.330	0.939

^a LV = number of latent variables; s_{CV} = [PRESS/(N_{obs} - 1 - N_{LV})]^{1/2}, where PRESS = Σ(y_{obs} - y_{pred})², N_{obs} = number of observations, and N_{LV} = number of selected latent variables; r²_{CV} = (SS - PRESS)/SS, where SS = Σ(y_{obs} - y_{mean})²; s_f = [CALSS/(N_{obs} - 1 - N_{LV})]^{1/2}, where CALSS = Σ(y_{obs} - y_{calc})²; r²_f = (SS - CALSS)/SS; F_{1, k} = stepwise *F*-value. ^b Number of selected latent variables.

only that all the examined compounds exert in that area more or less the same steric or electrostatic influence.

Figure 2 shows the CoMFA steric contours plotted using compounds **1** (blue), **13** (white), and **40** (red) as reference structures. The green and magenta polyhedra describe regions of space whose occupancy by the ligands respectively increases or decreases affinity to the MBR. The green contours surround the intermediate portion of 7-OCO-R₃ and 7-OSO₂-R₃ substituents (whenever present) with R₃ different from an aryl group. Notice that while the above "favorable" contours are in part occupied by the ester chain of compound **13**, they are also considerably far from the much less potent 7-keto analog **1**. The magenta contours are located in the corresponding areas of bulky and rigid aryl moieties, such as those present in compounds **19**, **25**, **39**, **40**, and **42**. These "unfavorable" contours are likely related to the presence of a sort of wall in the receptor cavity delimiting the volume accessible by the ligands. If this hypothesis is correct, compounds bearing at the 7-position lengthy alkanoyloxy chains (**11–13** and **15**) would

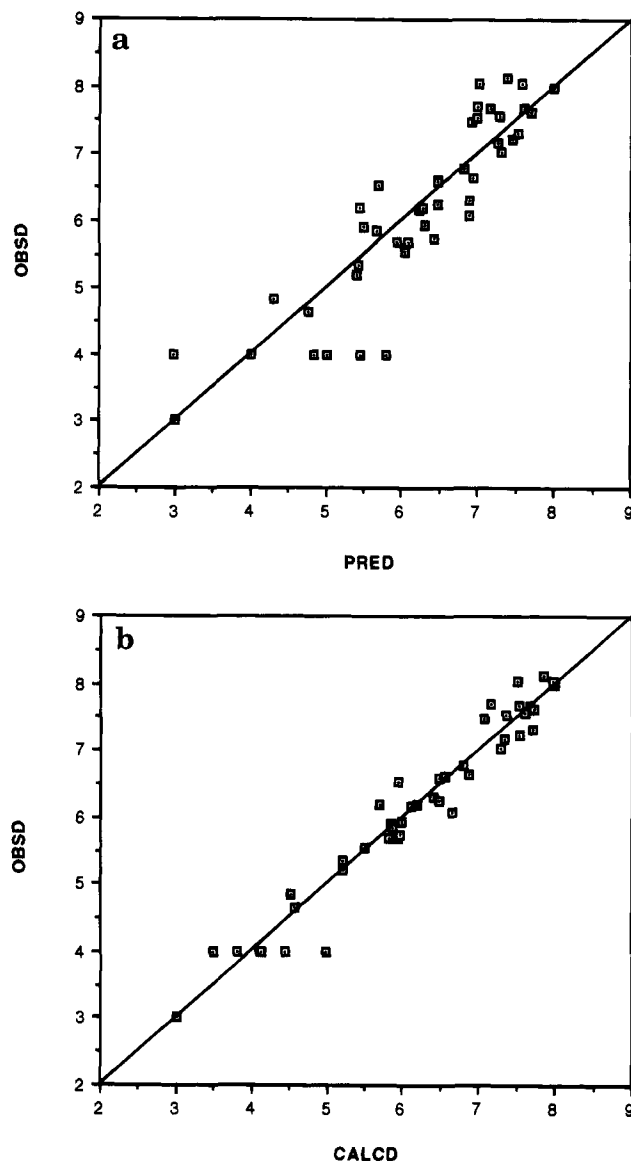


Figure 1. (a) Plot of observed versus predicted pI₅₀ values in the CoMFA cross-validation model. (b) Plot of observed versus calculated pI₅₀ values in the CoMFA calibration model.

retain high affinity by binding to the receptor in a folded conformation. Accordingly, the side chain of compound **13**, as those of its congeners, has been modeled in a conformation with the torsional angle O—C—C in a *gauche* disposition (see Figure 2 and Table 3).

In Figure 2, the presence of three very small magenta contours around the fused benzene ring can be hardly noticed. These contours might be related partly to the bulk of the substituents in the 2- and 3-positions in the ester derivatives **16–27** and **30** and partly to the particular disposition of the pendant phenyl ring in the ketones **1–7**.

Figure 3 shows various ligands embedded in the CoMFA electrostatic contour maps. The blue and red polyhedra describe regions where a high electron density within the ligand structure enhances or diminishes, respectively, affinity. In Figure 3, top, compounds **40** (green) and **8** (white) are shown for ease of interpretation. It can be seen that a part of the red contours runs parallel to the aromatic ring of **40** and surrounds at the same time an oxygen bound to the sulfur atom of **8**. According to the position of the red polyhedra, the loss of potency associated with 7-aryloxy substituents ap-

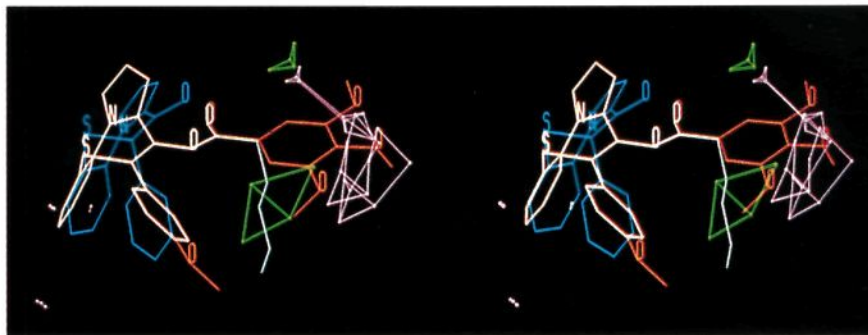


Figure 2. Stereopair picture of the CoMFA steric contour maps generated by interpolating at the 0.05 (green) and -0.05 (magenta) levels the pairwise products between the 3D-QSAR steric coefficients and the standard deviations of the associated energy variables. The green and magenta polyhedra correspond to regions where occupancy by the ligands respectively increases or decreases affinity. Compounds **1** (blue), **13** (white), and **40** (red) are shown as reference structures.

pears to be dependent not only on repulsive steric interactions with the receptor (see magenta contours in Figure 2) but also on the negative electrostatic potential existing above and under the plane of the aromatic rings. Additionally, the CoMFA model rationalizes the slightly lower affinity of the 7-(methylsulfonyl)oxy derivatives **8** and **38** with respect to the more potent 7-acetoxy derivatives **9** and **37** by associating the "additional" electronegative oxygen with a negative effect on affinity.

Figure 3, middle, shows the sulfo oxygens of compound **6** (white) surrounded by the red electrostatic CoMFA contours ("unfavorable" when they are near an electron rich substituent). This picture is consistent with the lowering of affinity consequent to oxidation of the endo-cyclic sulfur atom to sulfoxide or sulfone. We have already mentioned that the CoMFA electrostatic contour maps gave us suggestions of what conformation to choose for compounds **62** and **63**, depending on whether the 2'-fluorine atom is oriented toward or away from the endo-cyclic sulfur. It is the latter conformation which seems more favorable for binding affinity since the electronegative fluorine atom points toward a direction which "avoids" the above discussed red contours.

By looking at Figure 3, bottom, we can try to interpret the meaning of the blue and red polyhedra located in proximity of the fused benzene ring moieties. In this figure, compounds **29** (green), **4** (white), and **16** (violet) are superimposed. The presence of a chlorine atom at the 4-position of the benzothiazepine system leads to a modest increase of affinity. This effect is described by the blue contours located in the corresponding areas of the 4-chloro substituent in compound **29**. It is worth noting that the low-potent 7-keto analog **4** orients toward the same blue polyhedra two positively charged hydrogens belonging to the fused benzene ring.

The red polyhedra, just opposite to the 2- and 3-positions of compound **16**, take into account the about 100-fold drop of affinity observed when a chlorine, a trifluoromethyl, or a methoxy group is present at one of these positions.

The small red contour around the 4'-position of the pendant phenyl ring indicates that a methoxy group is responsible for a small decrease of affinity. However, such contour should not be overemphasized since there are several exceptions to this pattern (see couples **10/41**, **14/36**, **32/34**, and **21/23** where the 4'-methoxy derivative has a potency equal to or even higher than the corresponding 4'-desmethoxy derivative).

The blue contour in proximity of the pyrrole ring probably describes the detrimental effect on affinity caused by either electron-withdrawing groups on the benzene ring or by oxidation of the endo-cyclic sulfur. This would be consistent with the importance that our pharmacophore model²⁷ has been assigned to the electron density out of the plane of the pyrrole moiety.

Prediction of the Binding Affinity for Compounds of the Test Set. As already mentioned, compounds **62–68** (test set) allowed us to evaluate the efficiency of the derived CoMFA model in estimating binding affinity values for structures outside the training set.

The synthesis of the compounds belonging to the test set was actually planned before performing the CoMFA study. Most of them were chosen with the purpose of broadening the variance of the physicochemical properties characterizing the compounds of the training set. Specifically, through compounds **62–67** we wanted to further probe the receptor sites complementary to the 2'- and 4'-positions of the pendant phenyl ring and the 2- and 3-positions of the fused benzene ring. Compound **68** was instead designed by hypothesizing that additive effects of substituents on affinity would have led to an increased potency. In fact, **68** features two substituents, the 4-Cl and the 7-CON(CH₃)₂, which are independently present in the most potent compounds of the training set (**14**, **28**, and **36**).

Table 2 lists the observed pIC₅₀ values of the compounds belonging to the test set together with the corresponding pIC₅₀ values predicted through the CoMFA model. These values are also plotted in Figure 4.

The prediction of standard error, s_{pred} , was the parameter used to assess the predictive performance of the quantitative model ($s_{\text{pred}} = [\text{PRESS}/N_{\text{obs}}]^{1/2}$, where PRESS refers to predictions made for compounds of the test set and N_{obs} is the number of observations). The s_{pred} value from the seven predictions is quite good (0.536) and rather close to the s_{cv} value calculated from cross-validation (0.648).

Compound **68** was predicted to have a pIC₅₀ of 8.64. Although this ligand was found to possess a pIC₅₀ of 8.40, it nevertheless displays the highest affinity to the MBR among the so far investigated pyrrolobenzothiazepine derivatives.

Conclusions

The CoMFA method has been successfully applied in a set of recently described pyrrolobenzothiazepines

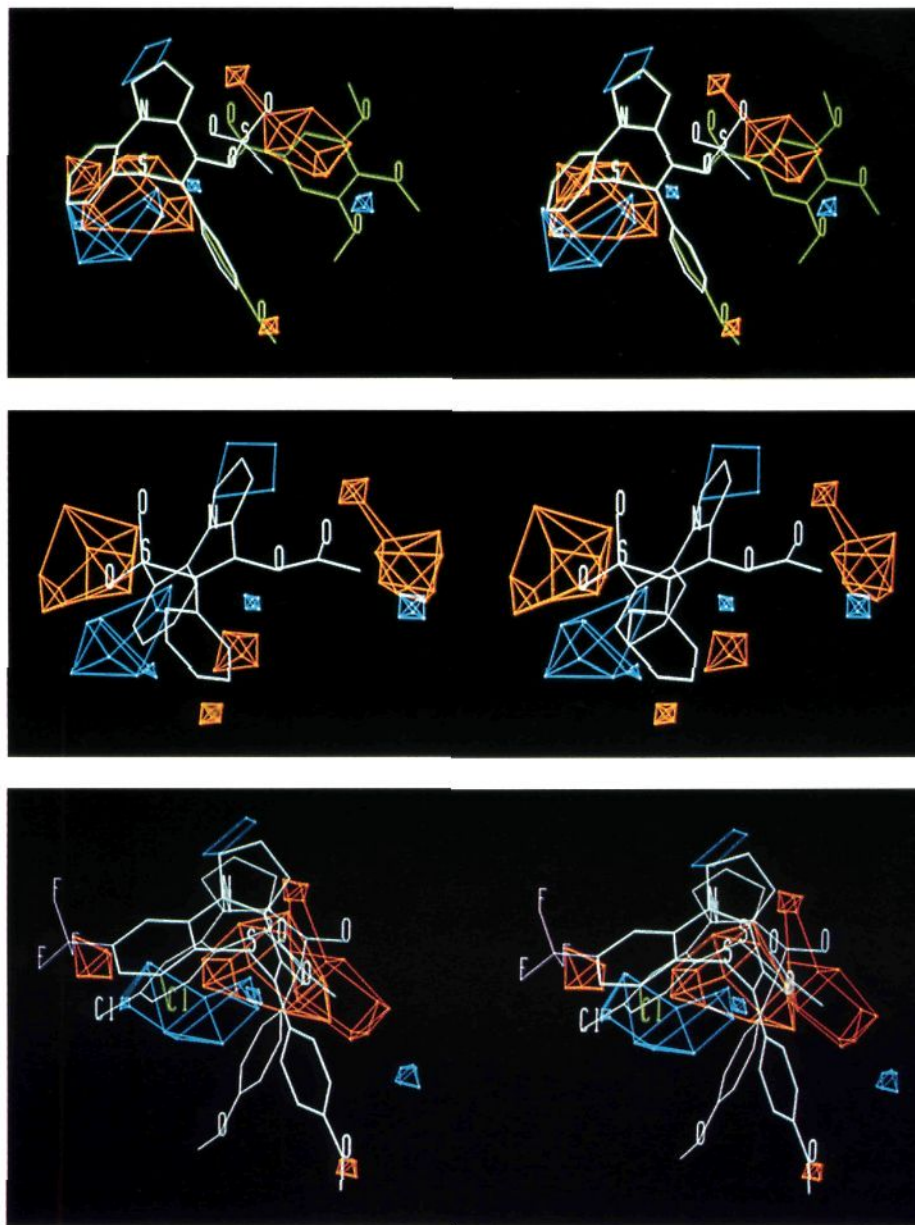


Figure 3. Stereopair picture of the CoMFA electrostatic contour maps generated by interpolating at the -0.05 (blue) and 0.05 (red) levels the pairwise products between the 3D-QSAR electrostatic coefficients and the standard deviations of the associated energy variables. The blue and red polyhedra correspond to regions where a high or poor electron density in the ligand is favorable or unfavorable, respectively, for affinity. (top) Compounds **40** (green) and **8** (white) are shown as an aid to the interpretation of the contours around the R_3 substituent. (middle) Compound **6** (white) is displayed with the negatively charged sulfo oxygens close to a part of the red contours. (bottom) Compounds **29** (green), **4** (white), and **16** (violet) are shown for an easy interpretation of the electronic effects exerted by substituents attached to the fused benzene ring.

binding to the MBR.²⁷ The resulting 3D-QSAR model derived from a training set of 42 ligands rationalizes the binding affinity in terms of steric and electrostatic properties. The CoMFA coefficient contour plots provide a self-consistent picture of the main chemical features responsible for pIC_{50} variations as well as suggestions about how to superimpose novel ligands. More importantly, the 3D-QSAR model has predicted the pIC_{50} values of seven newly synthesized compounds with an accuracy comparable to that obtained by applying the cross-validation procedure in a training set of 42 analogs.

Experimental Section

Melting points were determined using an Electrothermal 8103 apparatus and are uncorrected. IR spectra were taken

as Nujol mulls with Perkin-Elmer 398 and Perkin-Elmer FT 1600 spectrophotometers. 1H NMR spectra were recorded on a Bruker 200 MHz spectrometer with TMS as internal standard; the values of chemical shifts (δ) are given in ppm and the coupling constants (J) in Hz. All reactions were carried out in an atmosphere of dry nitrogen. Progress of the reaction was monitored by TLC on silica gel plates (Riedel-de-Haen; Art. 37341). Merck silica gel (Kieselgel 60) was used for chromatography (70–230 mesh) and flash chromatography (230–400 mesh) columns. Extracts were dried over Na_2SO_4 , and solvents were removed under reduced pressure. Elemental analyses were performed on a Perkin-Elmer 240C analyzer and are within $\pm 0.4\%$ of the theoretical values, unless otherwise noted. Yields refer to the purified products and are not optimized.

Bis(4-methyl-2-*N*-pyrrolylphenyl) Disulfide (44). To a suspension of bis(2-amino-4-methylphenyl) disulfide (0.57 g, 2.1 mmol) in glacial acetic acid (14 mL) was slowly added a

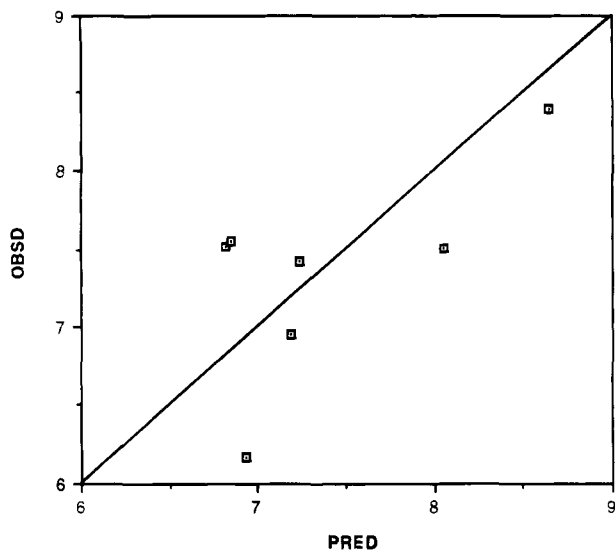


Figure 4. Plot of observed versus predicted pIC_{50} values for the compounds belonging to the test set.

solution of 2,5-dimethoxytetrahydrofuran (0.57, 4.3 mmol) in the same solvent (0.2 mL), and the resulting mixture was heated at 80 °C for 40 min. After cooling, the reaction mixture was concentrated *in vacuo* and the residue was taken up in $CHCl_3$, washed with saturated $NaHCO_3$ solution and H_2O , and dried. The solvent was removed, and the pasty residue was purified by flash column chromatography [$CHCl_3$ -petroleum ether (bp 60–80 °C), 1:2]. Recrystallization from petroleum ether (bp 60–80 °C) gave **44** (60% yield) as colorless needles (mp 50–55 °C). 1H NMR ($CDCl_3$): δ 2.33 (s, 6H, 2 CH_3), 6.33 (d, 4H, $J = 1.6$ Hz, β -pyrrole H), 6.76 (t, 4H, $J = 1.6$ Hz, α -pyrrole H), 7.02–7.38 (m, 6H, ArH). Anal. ($C_{22}H_{20}N_2S_2$) C, H, N.

Bis(5-methyl-2-N-pyrrolylphenyl) Disulfide (45). Compound **45** was prepared according to the procedure described for **44** starting from bis(2-amino-5-methylphenyl) disulfide (3.0 g, 21.5 mmol). Column chromatography ($CHCl_3$) and recrystallization from cyclohexane afforded **45** (35% yield) as other needles (mp 109–110 °C). 1H NMR ($CDCl_3$): δ 2.33 (s, 6H, 2 CH_3), 6.34 (t, 4H, $J = 1.8$ Hz, β -pyrrole H), 6.77 (t, 4H, $J = 1.8$ Hz, α -pyrrole H), 7.02–7.38 (m, 6H, ArH). Anal. ($C_{22}H_{20}N_2S_2$) C, H, N.

General Procedure for the Preparation of Esters 46–50. This procedure is illustrated for the preparation of α -[[4-methyl-2-(1*H*-pyrrol-1-yl)phenyl]thio]phenylacetic acid ethyl ester (**49**). A suspension of bis(4-methyl-2-*N*-pyrrolylphenyl) disulfide (**44**) (6.87 g, 18.2 mmol) in 135 mL of anhydrous EtOH was heated to reflux. Sodium borohydride (1.37 g, 36.4 mmol) was then added carefully, in portions, over 30 min. When adding stopped, the mixture was allowed to cool to room temperature and ethyl α -bromophenylacetate (8.84 g, 36.4 mmol) in 40 mL of anhydrous EtOH was slowly added. After stirring for 24 h at room temperature, the reaction mixture was reduced to one-half of the original volume *in vacuo* and poured into an equal volume of ice-water. The collected precipitate was purified by column chromatography (toluene) (50% yield). Recrystallization from EtOH afforded an analytical sample (mp 75–76 °C). 1H NMR ($CDCl_3$): δ 1.07 (t, 3H, $J = 7.2$ Hz, CH_2CH_3), 2.34 (s, 3H, CH_3), 4.01 (m, 2H, CH_2), 4.28 (s, 1H, CH), 6.34 (t, 2H, $J = 2.2$ Hz, β -pyrrole H), 6.92 (t, 2H, $J = 1.9$ Hz, α -pyrrole H), 7.03–7.64 (m, 8H, ArH). IR: 1750 cm^{-1} . Anal. ($C_{21}H_{21}NO_2S$) C, H, N.

This procedure was repeated with bis(5-methyl-2-*N*-pyrrolylphenyl) disulfide (**45**) to give the ester **50** and with bis(2-*N*-pyrrolylphenyl) disulfide (**43**) for reaction with α -bromo-*o*-fluorophenylacetate, α -bromo-*p*-chlorophenylacetate, or α -bromo-*p*-fluorophenylacetate to give the esters **46–48**, respectively. Yields and analytical data are given in Table 4. The IR and 1H NMR spectra are consistent with the assigned structures.

General Procedure for the Preparation of Acids 51–55. This procedure is illustrated for the preparation of α -[[4-

methyl-2-(1*H*-pyrrol-1-yl)phenyl]thio]phenylacetic acid (**54**). The ester **49** (2.95 g, 8.38 mmol) was dissolved in 22 mL of EtOH, and 5% aqueous NaOH (22 mL) was slowly added. The reaction mixture was stirred at 40 °C for 1 h, concentrated, and acidified with 6 N HCl to pH 3–4. The mixture was extracted with $CHCl_3$, and the organic phase was washed with brine, dried, and concentrated. The crude compound was recrystallized from cyclohexane (56% yield) (mp 125–127 °C). 1H NMR ($DMSO-d_6$): δ 2.32 (s, 3H, CH_3), 4.83 (s, 1H, CH), 6.26 (t, 2H, $J = 1.9$ Hz, β -pyrrole H), 6.93 (t, 2H, $J = 1.9$ Hz, α -pyrrole H), 7.14–7.96 (m, 8H, ArH), 13.04 (s, 1H, COOH, D_2O). IR: 1710 cm^{-1} . Anal. ($C_{19}H_{17}NO_2S$) C, H, N.

Similarly acids **51–53** and **55** were prepared starting from the related esters **46–48** and **50**. Yields and analytical data are reported in Table 4. The IR and 1H NMR spectra are consistent with the assigned structures.

General Procedure for the Preparation of Ketones 56–60. This procedure is illustrated for the preparation of 6-(*p*-chlorophenyl)pyrrolo[2,1-*d*][1,5]benzothiazepin-7(6*H*)-one (**57**). To a well-stirred solution of **52** (0.67 g, 1.94 mmol) in anhydrous CH_2Cl_2 (6 mL) was slowly added a suspension of PCl_5 (0.6 g, 2.92 mmol) in the same solvent (5.5 mL). The resulting mixture was heated at 60 °C for 5 h and allowed to stir at room temperature for 48 h. The solvent was removed under reduced pressure, and the oily dark residue was treated with Et_2O . The ethereal solution was washed with 5% aqueous NaOH and water, dried, and concentrated to yield a residue that was purified by column chromatography using $CHCl_3$ -petroleum ether (bp 60–80 °C), 1:1, as the eluent. The title compound was obtained as a white solid (48% yield). An analytical sample was recrystallized from EtOH (mp 162–163 °C). 1H NMR ($CDCl_3$): δ 4.67 (s, 1H, H-6), 6.37 (dd, 1H, $J = 2.2$ and 3.4 Hz, H-9), 6.85–7.36 (m, 10H, ArH, H-8, and H-10). IR: 1649 cm^{-1} . Anal. ($C_{18}H_{12}ClNOS$) C, H, N.

Similarly **56** and **58–60** were prepared starting from related acids **51** and **53–55**. Yields and analytical data are given in Table 4.

56. 1H NMR ($CDCl_3$): δ 4.96 (s, 1H, H-6), 6.49 (t, 1H, $J = 3.4$ Hz, H-9), 6.86–7.53 (m, 10H, ArH, H-8, and H-10). IR: 1649 cm^{-1} . Anal. ($C_{18}H_{12}FNOS$) C, H, N; calcd, 4.53; found, 5.05.

58. 1H NMR ($CDCl_3$): δ 4.81 (s, 1H, H-6), 6.47 (t, 1H, $J = 3.3$ Hz, H-9), 6.78–7.46 (m, 10H, ArH, H-8, and H-10). IR: 1649 cm^{-1} . Anal. ($C_{18}H_{12}FNOS$) C, H, N.

59. 1H NMR ($CDCl_3$): δ 2.29 (s, 3H, CH_3), 4.70 (s, 1H, H-6), 6.39 (t, 1H, $J = 3.6$ Hz, H-9), 6.84–7.36 (m, 10H, ArH, H-8, and H-10). IR: 1640 cm^{-1} . Anal. ($C_{19}H_{15}NOS$) C, H, N.

60. 1H NMR ($CDCl_3$): δ 2.19 (s, 3H, CH_3), 4.75 (s, 1H, H-6), 6.40 (t, 1H, $J = 3.2$ Hz, H-9), 6.99–7.41 (m, 10H, ArH, H-8, and H-10). IR: 1650 cm^{-1} . Anal. ($C_{19}H_{15}NOS$) C, H, N.

General Procedure for the Preparation of Compounds 62–68. This procedure is illustrated for the preparation of 7-acetoxy-6-(*p*-chlorophenyl)pyrrolo[2,1-*d*][1,5]benzothiazepine (**64**). To a stirred suspension of potassium hydride (0.1 g, 2.45 mmol) in anhydrous tetrahydrofuran (3 mL) was slowly added a solution of compound **57** (0.8 g, 2.45 mmol) in 9 mL of the same solvent. After the mixture was stirred for 24 h at room temperature, a solution of acetyl chloride (0.19 g, 2.45 mmol) in anhydrous tetrahydrofuran (1 mL) was added dropwise and the mixture stirred for additional 5 h at room temperature. The reaction mixture was poured onto crushed ice and extracted with Et_2O . The combined organic layers were dried and evaporated. The residue purified by column chromatography (toluene) afforded **64** in 67% yield which, after crystallization from EtOH, melted at 172–174 °C (white crystals). 1H NMR ($CDCl_3$): δ 1.96 (s, 3H, CH_3), 6.41 (t, 1H, $J = 3.0$ Hz, H-9), 6.61 (d, 1H, $J = 4.4$ Hz, H-8), 7.23–7.69 (m, 9H, ArH and H-10). IR: 1770 cm^{-1} . Anal. ($C_{20}H_{14}ClNO_2S$) H, N; C: calcd, 65.30; found, 65.80.

Similarly **62**, **63**, and **65–68** were obtained. Starting compounds, reaction times after the proper acid chloride adding, column chromatography eluents, yields, melting points, and spectral data are as follows.

62:56, 12 h, CH_2Cl_2 -cyclohexane, 3:1, 15% yield, mp 122–124 °C (white crystals from EtOH). 1H NMR ($CDCl_3$): δ 1.92 (s, 3H, CH_3), 6.42 (t, 1H, $J = 3.0$ Hz, H-9), 6.62 (dd, 1H, $J =$

1.7 and 3.8 Hz, H-8), 7.03–7.63 (m, 9H, ArH and H-10). IR: 1780 cm⁻¹. Anal. (C₂₀H₁₄FNO₂S) C, H, N.

63:56, 12 h, CHCl₃, 54% yield, mp 132–134 °C (green crystals from EtOH). ¹H NMR (CDCl₃): δ 2.73 (s, 3H, CH₃), 2.82 (s, 3H, CH₃), 6.41 (t, 1H, J = 3.0 Hz, H-9), 6.60 (dd, 1H, J = 2.0 and 3.9 Hz, H-8), 6.97–7.60 (m, 9H, ArH and H-10). IR: 1735 cm⁻¹. Anal. (C₂₁H₁₇FN₂O₂S) C, H, N.

65:58, 1 h, CHCl₃, 59% yield, mp 157–159 °C (green microcrystals from EtOH). ¹H NMR (CDCl₃): δ 1.95 (s, 3H, CH₃), 6.42 (d, 1H, J = 3.1 Hz, H-9), 6.62 (dd, 1H, J = 1.9 and 3.9 Hz, H-8), 6.97–7.60 (m, 9H, ArH and H-10). IR: 1760 cm⁻¹. Anal. (C₂₀H₁₄FNO₂S) C, H, N.

66:59, 4 h, CHCl₃, 63% yield, mp 132–134 °C (white crystals from EtOH). ¹H NMR (CDCl₃): δ 1.91 (s, 3H, COCH₃), 2.34 (s, 3H, CH₃), 6.38 (t, 1H, J = 3.0 Hz, H-9), 6.58 (d, 1H, J = 1.7, H-8), 7.08–7.54 (m, 9H, ArH and H-10). IR: 1765 cm⁻¹. Anal. (C₂₁H₁₇NO₂S) C, H, N.

67:60, 2 h, CHCl₃, 45% yield, mp 126–127 °C (white crystals from EtOH). ¹H NMR (CDCl₃): δ 1.88 (s, 3H, COCH₃), 2.31 (s, 3H, CH₃), 6.32 (t, 1H, J = 3.1 Hz, H-9), 6.52 (dd, 1H, J = 1.6 and 3.7 Hz, H-8), 7.04 (d, 1H, J = 2.0 Hz, H-10), 7.16–7.46 (m, 8H, ArH). IR: 1779 cm⁻¹. Anal. (C₂₁H₁₇NO₂S) C, H, N.

68:61,¹ 4 h, CH₂Cl₂–petroleum ether (bp 60–80 °C), 2:1, 57% yield, mp 178–180 °C (green crystals from EtOH). ¹H NMR (CDCl₃): δ 2.75 (s, 3H, CH₃), 2.93 (s, 3H, CH₃), 6.40 (t, 1H, J = 3.3 Hz, H-9), 6.60 (dd, 1H, J = 2.0 and 3.9 Hz, H-8), 7.08 (d, 1H, J = 3.2 Hz, H-10), 7.20–7.72 (m, 8H, ArH). IR: 1752 cm⁻¹. Anal. (C₂₁H₁₇ClN₂O₂S) C, H, N.

Binding Assays. Male CRL:CD(SD)BR rats (Charles River Italia, Calco, BG, Italy), weighing about 150 g, were used in these experiments. Before being killed by decapitation (unanes-
thetized), the rats had been housed in groups of five in plastic cages, kept under standard conditions (room temperature, 21 ± 1 °C; relative humidity, 55 ± 10%; 12/12 h light–dark cycle), and given tap water and food pellets *ad libitum*. After decapitation, the brains were rapidly removed from the skulls and dissected out into various anatomically recognizable areas. Cortices were homogenized in about 50 volumes of ice-cold phosphate-buffered saline, 50 mM, pH 7.4, using an Ultra Turrax TP-1810 homogenizer (2 × 20 s) and centrifuged at 50000g for 10 min. The pellet was then washed three times more by resuspensions in fresh buffer and centrifugations as before. The last pellet was resuspended just before the binding assay.

For mitochondrial benzodiazepine binding,²⁴ 10 mg of original wet tissue weight was incubated with 1 nM [³H]PK 11195 (specific activity, 85.8 Ci/mmol; NEN) in 1 mL final volume for 120 min at 4 °C in the presence of 8–12 increasing concentrations of drugs. Nonspecific binding was determined by using 1 μM PK 11195.

Incubations were stopped by rapid filtration under vacuum through GF/B fiber filters which were then washed with 12 mL of ice-cold buffer and counted in 8 mL of Filter Count (Packard) in a liquid scintillation spectrometer (LKB; Model Rakbeta 1214) with a counting efficiency of about 56%. IC₅₀s were determined by nonlinear fitting⁴⁷ of binding inhibition curves, using the Allfit program running on an IBM AT personal computer. Each point was the mean of triplicate samples.

Acknowledgment. This work was supported by a grant from MURST, Rome.

References

- Anholt, R. R. H.; Pedersen, P. L.; De Souza, F. B.; Snyder, S. H. The peripheral-type benzodiazepine receptor. *J. Biol. Chem.* **1986**, *261*, 576–583.
- Basile, A. S.; Skolnick, P. Subcellular localization of "peripheral-type" binding sites for benzodiazepines in rat brain. *J. Neurochem.* **1986**, *46*, 305–308.
- O'Beirne, G. B.; Williams, D. C. The subcellular location in rat kidney of the peripheral benzodiazepine receptor. *Eur. J. Biochem.* **1988**, *175*, 413–421.
- Sprengler, R.; Werner, P.; Seeburg, P. H. Molecular Cloning and expression of cDNA encoding a peripheral-type benzodiazepine receptor. *J. Biol. Chem.* **1989**, *264*, 20415–20421.
- Doble, A.; Benavides, J.; Ferris, O.; Bertrand, P.; Menager, J.; Vaucher, N.; Burgevin, M. C.; Uzan, A.; Guérémy, C.; Le Fur, G. Dihydropyridine and peripheral type benzodiazepine binding sites: subcellular distribution and molecular size determination. *Eur. J. Pharmacol.* **1989**, *161*, 197–202.
- Verma, A.; Snyder, S. H. Peripheral-type benzodiazepine receptors. *Annu. Rev. Pharmacol. Toxicol.* **1989**, *29*, 307–322.
- Katz, Y.; Amiri, Z.; Weizman, A.; Gavish, M. Identification and distribution of peripheral benzodiazepine binding sites in male rat genital tract. *Biochem. Pharmacol.* **1990**, *40*, 817–820.
- McEnery, M. W.; Snowman, A. M.; Trifletti, R. R.; Snyder, S. H. Isolation of the mitochondrial benzodiazepine receptor: association with the voltage dependent anion channel and the adenine nucleotide carrier. *Proc. Natl. Acad. Sci. U.S.A.* **1992**, *89*, 3170–3174.
- Zavala, F.; Haumont, J.; Lenfant, M. Interaction of benzodiazepines with mouse macrophages. *Eur. J. Pharmacol.* **1984**, *106*, 561–566.
- Mestre, M.; Carriot, T.; Belin, C.; Uzan, A.; Renault, C.; Dubroeuq, M. C.; Guérémy, C.; Le Fur, G. Electrophysiological and pharmacological characterization of peripheral benzodiazepine receptors in guinea pig heart preparation. *Life Sci.* **1984**, *35*, 953–962.
- Wang, J. K. T.; Morgan, J. I.; Spector, S. Benzodiazepines that bind at peripheral sites inhibit cell proliferation. *Proc. Natl. Acad. Sci. U.S.A.* **1984**, *81*, 3770–3772.
- Anholt, R. R. H.; De Souza, E. B.; Oster-Granite, M. L.; Snyder, S. H. Peripheral-type benzodiazepine receptors: autoradiographic localization in whole-body sections of neonatal rats. *J. Pharmacol. Exp. Ther.* **1985**, *233*, 517–526.
- Ruff, M. R.; Pert, C. B.; Weber, R. J.; Wahl, L. M.; Paul, S. M. Benzodiazepine receptor-mediated chemotaxis of human monocytes. *Science* **1985**, *229*, 1281–1283.
- Grupp, I. L.; Frevich, J. F.; Matlib, M. A. Benzodiazepine Ro 5-4854 increases coronary flow. *Eur. J. Pharmacol.* **1987**, *143*, 143–147.
- Basile, A. S.; Lueddens, H. W. M.; Skolnick, P. Regulation of renal peripheral benzodiazepine receptors by anionic transport inhibitors. *Life Sci.* **1988**, *42*, 715–726.
- Moreno-Sanchez, R.; Hogue, B. A.; Bravo, C.; Newman, A. H.; Basile, A. S.; Chiang, P. K. Inhibition of substrate oxidation in mitochondria by the peripheral-type benzodiazepine receptor ligand AHN 086. *Biochem. Pharmacol.* **1990**, *41*, 1479–1484.
- Amsterdam, A.; Sun Suh, B. An inducible functional peripheral benzodiazepine receptor in mitochondria of steroidogenic granulosa cells. *Endocrinology* **1991**, *129*, 503–510.
- Papadopoulos, V.; Guarneri, P.; Krueger, K. E.; Guidotti, A.; Costa, E. Pregnenolone biosynthesis in C6 glioma cell mitochondria: regulation by a mitochondrial diazepam binding inhibitor receptor. *Proc. Natl. Acad. Sci. U.S.A.* **1992**, *89*, 5113–5117.
- Guarneri, P.; Papadopoulos, V.; Pan, B.; Costa, E. Regulation of pregnenolone synthesis in C6-2B glioma cells by 4'-chlorodiazepam. *Proc. Natl. Acad. Sci. U.S.A.* **1992**, *89*, 5118–5122.
- Langer, S. Z.; Arbilla, S.; Scatton, B.; Niddam, R.; Dubois, A. Receptors involved in the mechanism of action of zolpidem. In *Imidazopyridines in sleep disorders*; Sauvaget, J. P., Langer, S. Z., Morselli, P. L., Eds.; Raven Press: New York, 1988; pp 55–70.
- Autu, J.; Romeo, E.; Kozikowski, A. P.; Ma, D.; Costa, E.; Guidotti, A. Participation of mitochondrial DBI receptors in the anticonvulsant, antineophobic, and anticonvulsant action of 2-aryl-3-indoleacetamide and imidazopyridine derivatives. *J. Pharmacol. Exp. Ther.* **1993**, *265*, 649–656.
- Kozikowski, A. P.; Ma, D.; Brewer, J.; Sun, S.; Costa, E.; Romeo, E.; Guidotti, A. Chemistry, binding affinities and behavioral properties of a new class of "antineophobic" mitochondrial DBI receptor complex (mDRC) ligands. *J. Med. Chem.* **1993**, *36*, 2908–2920.
- Shoemaker, K.; Boles, R. G.; Horst, W. D.; Yamamura, H. I. Specific high-affinity binding sites for ³H Ro 5-4864 in rat brain and kidney. *J. Pharmacol. Exp. Ther.* **1983**, *225*, 61–69.
- Gobbi, M.; Barone, D.; Mennini, T.; Garattini, S. Diazepam and desmethyl-diazepam differ in their affinities and efficacies at "central" and "peripheral" benzodiazepine receptors. *J. Pharm. Pharmacol.* **1987**, *39*, 388–391.
- Bond, P. A.; Cundall, R. L.; Rolfe, B. 3H diazepam binding to human granulocytes. *Life Sci.* **1985**, *37*, 11–16.
- Nacci, V.; Fiorini, I.; Garofalo, A.; Cagnotto, A. Research on compounds with psychotropic activity. IX. Synthesis of 6-p-methoxyphenylpyrrolo[2,1-d][1,5]benzothiazepines and evaluation of their affinity for BDZ and GABA receptor subtypes. *Farmacol.* **1990**, *45*, 545–557.
- Fiorini, I.; Nacci, V.; Ciani, S. M.; Garofalo, A.; Campiani, G.; Savini, L.; Novellino, E.; Greco, G.; Bernasconi, P.; Mennini, T. Novel ligands specific for mitochondrial benzodiazepine receptors: 6-arylpyrrolo[2,1-d][1,5]benzothiazepine derivatives. Synthesis, structure-activity relationships and molecular modeling studies. *J. Med. Chem.* **1994**, *37*, 1427–1438.

- (28) Baulieu, E.-E.; Robel, P. J. Neurosteroids: a new brain function? *J. Steroid Biochem. Mol. Biol.* **1990**, *37*, 395-403.
- (29) Jung-Testas, I.; Hu, Z.; Baulieu, E.-E. Neurosteroids: biosynthesis of pregnenolone and progesterone in primary cultures of rat glial cells. *Endocrinology* **1989**, *125*, 2083-2091.
- (30) Puia, G.; Santi, M. R.; Vincini, S. Neurosteroids act on recombinant human GABA_A receptors. *Neuron* **1990**, *4*, 759-765.
- (31) Tallmann, J. F.; Thomas, J. W.; Gallager, D. W. GABAergic modulation of benzodiazepine binding site sensitivity. *Nature (London)* **1978**, *274*, 383-385.
- (32) Costa, E.; Guidotti, A. Diazepam binding inhibitor (DBI): a peptide with multiple biological actions. *Life Sci.* **1991**, *49*, 325-344.
- (33) Marangos, P. J.; Patel, J.; Boulenger, J. P.; Clark-Roseberg, R. Characterization of peripheral-type benzodiazepine binding sites in brain using ³H-Ro 5-4864. *Mol. Pharmacol.* **1982**, *22*, 26-32.
- (34) Le Fur, G.; Perrier, J.; Uzan, A.; Renault, C.; Dubroeuq, M. C.; Guérémy, C. Peripheral benzodiazepine binding sites: effect of PK 11195, 1-(2-chlorophenyl)-N-methyl-N-(1-methylpropyl)-3-isoquinolinecarboxamide I. In vitro studies. *Life Sci.* **1983**, *32*, 1839-1847.
- (35) Le Fur, G.; Guilloux, F.; Rufat, P.; Benavides, J.; Uzan, A.; Renault, C.; Dubroeuq, M. C.; Guérémy, C. Peripheral benzodiazepine binding sites: effect of PK 11195, 1-(2-chlorophenyl)-N-methyl-N-(1-methylpropyl)-3-isoquinolinecarboxamide II. In vivo studies. *Life Sci.* **1983**, *32*, 1849-1856.
- (36) Cramer, R. D., III; Patterson, D. E.; Bunce, J. D. Comparative Molecular Field Analysis (CoMFA) 1. Effects of shape on binding of steroids to carrier proteins. *J. Am. Chem. Soc.* **1988**, *110*, 5959-5967.
- (37) DePriest, S. A.; Mayer, D.; Naylor, C. B.; Marshall, G. R. 3D-QSAR of angiotensin-converting enzyme and thermolysin inhibitors: a comparison of CoMFA models based on deduced and experimentally determined active site geometries. *J. Am. Chem. Soc.* **1993**, *115*, 5372-5384.
- (38) SYBYL Molecular Modeling System, Version 5.41; TRIPOS Associates: St. Louis, MO.
- (39) Vinter, J. G.; Davis, A.; Saunderson, M. R.; Strategic approaches to drug design. 1. An integrated software framework for molecular modeling. *J. Comput.-Aided Mol. Des.* **1987**, *1*, 31-55.
- (40) MOPAC, Version 5.00. Quantum Chemistry Program Exchange No. 455, 1989.
- (41) Dewar, M. J. S.; Thiel, W. Ground states of molecules. 38. The MNDO method. Approximations and parameters. *J. Am. Chem. Soc.* **1977**, *99*, 4899-4907.
- (42) Wold, S.; Ruhe, A.; Wold, H.; Dunn, W. J. The covariance problem in linear regression. The partial least squares (PLS) approach to generalized inverses. *SIAM J. Sci. Stat. Comput.* **1984**, *5*, 735-743.
- (43) Cramer, R. D., III; Bunce, J. D.; Patterson, D. E.; Frank, I. E. Crossvalidation, bootstrapping, and partial least squares compared with multiple regression in conventional QSAR studies. *Quant. Struct.-Act. Relat.* **1988**, *7*, 18-25.
- (44) Palmer, P. J.; Trigg, R. B.; Warrington, J. V. Benzothiazepines as antituberculous agents. *J. Med. Chem.* **1971**, *14*, 248-251.
- (45) Lawrence, J. P. Ger. Offen. 2, 503, 164, Aug 1975; *Chem. Abstr.* **1975**, *83*, 205904h.
- (46) Nacci, V.; Filacchioni, G.; Stefancich, G. Ricerche su sostanze ad attività psicotropa. Nota III. Sintesi di un nuovo sistema eterociclico: la 4H-pyrrolo[2,1-c][1,4]benzotiazepina. (Compounds with psychotropic activity. III. Synthesis of a new heterocyclic system. 4H-pyrrolo[2,1-c][1,4]benzothiazine.) *Farmaco, Ed. Sci.* **1973**, *28*, 545-555.
- (47) Munson, P. G.; Roadbard, D. *Computers in Endocrinology*; Raven Press: New York, 1984; pp 117-145.